Journal of Polymer Science

WILEY

JOURNAL OF POLYMER SCIENCE

RESEARCH ARTICLE OPEN ACCESS

Synthesis of HDPE-*b*-*i*PP Diblock Copolymers via Subsequent Coordintive Chain-Transfer Polymerization and Their Use as Compatibilizers for HDPE/*i*PP Blends

André Dickert | Patrick Wolff | Winfried P. Kretschmer | Rhett Kempe

Lehrstuhl Anorganische Chemie II–Katalysatordesign, Sustainable Chemistry Centre, Universität Bayreuth, Bayreuth, Germany

Correspondence: Winfried P. Kretschmer (winfried.kretschmer@uni-bayreuth.de) | Rhett Kempe (kempe@uni-bayreuth.de)

Received: 7 February 2025 | **Revised:** 18 May 2025 | **Accepted:** 19 May 2025

Funding: This work was supported by University of Bayreuth.

Keywords: block copolymers | CCTP | circular polyolefins | compatibilizer | polymer blends

ABSTRACT

An envisioned circular economy of commonly used polymers, high-density polyethylene (HDPE) and isotactic polypropylene (*i*PP), is challenging due to their immiscibility with almost all other plastics. Therefore, highly effective compatibilizers and synthetic protocols permitting their large-scale production are highly desirable. Herein, we report the efficient one-pot synthesis of strictly linear HDPE-*b*-*i*PP diblock copolymers achieved by coordinative chain transfer polymerization (CCTP). Various diblock copolymers with short and very narrow distributed HDPE ($M_n = 1400–2400\,g \times mol^{-1}$; $Đ = 1.4$) and long *i*PP segments were synthesized and used to compatibilize HDPE/*i*PP blends. The synthesized block copolymers differ in their overall molecular weights ($M_n = 10{,}600–60{,}600\,g \times mol^{-1}$) by varying the *i*PP segment, whereas the HDPE block was kept in a narrow range. Block copolymers with a molecular weight from $M_n = 23{,}000–39{,}000\,g \times mol^{-1}$ are competitive or outperform commercial compatibilizers, INFUSE™ and INTUNE™, with the highest efficiency in compatibilizing 30/70 (wt./wt.) HDPE/*i*PP blends by a 5 wt.-% copolymer addition. SEM studies revealed that after adding the diblock copolymer, HDPE core shell structures were formed, and the HDPE particle size decreases compared to the neat blend, avoiding HDPE particles from debonding during tensile deformation tests.

1 | Introduction

Due to their superior properties, polyethylene (PE) and isotactic polypropylene (*i*PP) are the most widely used polymers in the world [1]. However, their high demand and poor biodegradability inevitably lead to an increase in plastic waste, making a circular economy of these polymers necessary [2]. Despite their very similar molecular structures, PE and *i*PP are not miscible with each other, undergo macrophase separation, and turn recycling in the form of polymer blends due to their poor mechanical properties into a challenging task [3]. Copolymers containing HDPE and/or *i*PP block architectures as compatibilizers can significantly improve the mechanical properties of polymer blends even at very low concentrations [4]. They can reduce or overcome the domain formation and restore the original properties of the major component of the blend. Several kinds of HDPE/*i*PP compatibilizers have been described in literature [5], starting from diblock [6], triblock [7], linear multiblock [8], star like [9], grafted [10, 11], cycles [12] and random [13] copolymers (Figure 1A). Due to their promising results in HDPE/*i*PP compatibilizing and recycling, the research over the last decades has focused on PE and/or *i*PP grafted or multiblock copolymers and has led to the commercialization of a compatibilizer by the DOW Chemical

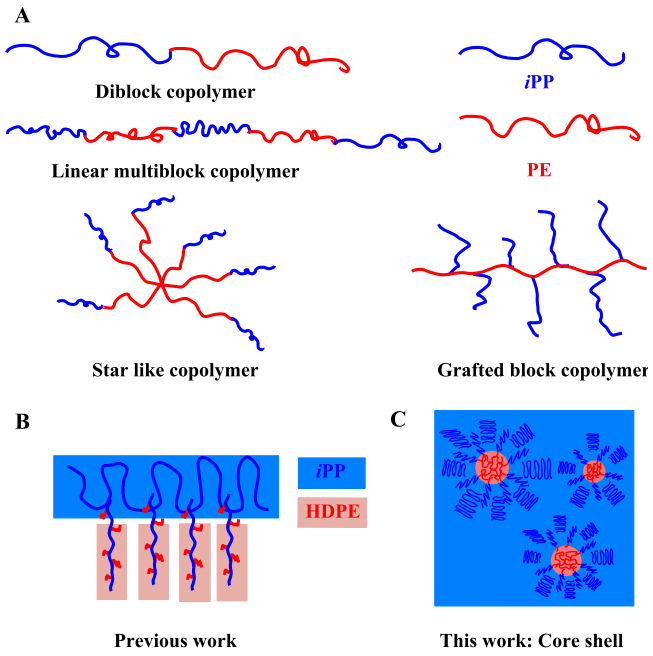

FIGURE 1 | (A) Selected nonreactive HDPE-*i*PP block copolymer compatibilizers. (B) Previous work: Illustration of an immiscible HDPE/*i*PP polymer-polymer interface stabilized by a HDPE grafted *i*PP block copolymer, which cocrystallizes in both domains. (C) This work: HDPE-core-*i*PP-shell formation in an *i*PP matrix, stabilized by a HDPE-*b*-*i*PP diblock copolymer.

Company under the trade name INFUSE™ [14]. INFUSE™ is an olefin multiblock copolymer (OBC) with alternating blocks of hard (rigid) and soft (elastomeric) segments. INFUSE™ consists of hard PE units with low α-olefin incorporation (HDPE) and soft randomly distributed ethylene-α-olefin copolymers (LLDPE) and is produced by chain shuttling technology [15]. Chain shuttling polymerization is a one-pot dual-catalyst approach for producing block copolymers by shuttling polymer chains between them.

PE-*b*-*i*PP diblock compatibilizers, especially hard-hard diblock copolymers, have been less investigated so far, and the research has mainly focused on two long and/or equal chain lengths because it is believed that short chains can be easily pull out [8a, 16]. A typical commercially available diblock compatibilizer with long chains is produced by the DOW Chemical Company under the trade name INTUNE™ (Table S1) [17]. INTUNE™ is an *i*PP-EP block copolymer consisting of a crystalline *i*PP and a randomly distributed ethylene-propene (EP) block [14c, 18], allowing both hard-hard and hard-soft variations, by softening or hardening the ethylene block through more or less propene incorporation. INTUNE™ is produced by coordinative chain transfer polymerization (CCTP) [15b, 19]. CCTP is a degenerative chain transfer process in which one catalyst molecule forms numerous macromolecules in a highly controlled fashion. A polymer chain can reversibly transmetalate between a transition metal-based catalyst (growing state) and a main group metal alkyl (dormant state), such as triethylaluminum ($AlEt_3$), diethylzinc ($ZnEt_2$) or dialkylmagnesium (MgR_2). Recently, we have applied this process to synthesize grafted HDPE chains on *i*PP back bones and have used these block copolymers to compatibilize HDPE in an *i*PP matrix (Figure 1B) [11].

Herein, we report the synthesis of semicrystalline, hard-hard HDPE-*b*-*i*PP diblock copolymers with variable molecular weight, consisting of a short very narrowly distributed HDPE chain and an *i*PP chain of adjustable length. A one-pot synthesis protocol is used, applying CCTP with two sequentially polymerized olefins. A carefully selected combination of depleted MAO (d-MAO) as activator, triethylaluminum ($AlEt_3$) as chain transfer agent (CTA) and two highly active catalysts that act sequentially with opposite α-olefin selectivities enables the efficient bulk synthesis of HDPE-*b*-*i*PP diblock copolymers. These copolymers can compatibilize HDPE/*i*PP blends permitting recycling of such plastic mixtures and are competitive with or outperform commercially available compatibilizers. Mechanistic investigations suggest a core shell mechanism for compatibilization (Figure 1C), which inhibits the crystallization-induced crack formation on polymer interfaces.

2 | Results and Discussion

2.1 | Synthesis of the HDPE-*b*-*i*PP Diblock Copolymers

The synthesis of our HDPE-*b*-*i*PP diblock copolymers is shown in Figure 2. The polymers are synthesized in a one-pot process, consisting of two sequential steps that involve two different olefins and catalysts: a guanidinato trimethanido zirconium(IV) (Zr^I) [20] and an *ansa*-bis(indenyl) dichlorido zirconium(IV) (Zr^{II}) [21]. The first catalyst (Zr^I), developed by our group, is highly reversible in the CCTP of ethylene, has a high $AlEt_3$ tolerance for a broadly tunable chain length, and exhibits a very fast chain transfer to aluminum, allowing the simultaneous growth of all alkyl groups to $Al(HDPE)_3$ with a very narrow polydispersity (Table S2; Figures S1 and S2), but it does not homopolymerize propylene. The second catalyst (Zr^{II}) has a very good α-olefin response, matches the high $AlEt_3$ tolerance of Zr^I, and polymerizes propylene in an isotactic fashion via irreversible CCTP [22]. Both catalysts can be activated with d-MAO.

In Step I, the Zr^I ethylene CCTP catalyst is used to synthesize linear aluminum terminated HDPE [$Al(HDPE)_3$] with a flexible chain length, whereas the discrimination of propylene homopolymerization avoids by-products in Step II. The chain length of the HDPE can be adjusted by the triethylaluminum concentration and fine-tuned by changing the amount of ethylene consumed. For the synthesis of HDPE-*b*-*i*PP diblock copolymers, a HDPE chain length above the entanglement range, $1200\,g \times mol^{-1}$, and below the precipitation point of $Al(HDPE)_3$ in toluene at 70°C, $2800\,g \times mol^{-1}$, was chosen.

In Step II, the monomer feed is switched to propylene and the Zr^{II} catalyst is added to the reaction mixture. Zr^{II} stereoselectively polymerizes propylene in an isotactic manner via irreversible CCTP in the presence of trialkylaluminum (AlR_3) and elongates the ethylene polymeryl chains with an *i*PP block of adjustable chain length to $(HDPE\text{-}iPP)_nAl(HDPE)_{3-n}$ ($n = 1, 2, 3$). The chain length of the *i*PP block is specified by varying the trialkylaluminum concentration, the propylene pressure, and polymerization temperature. Although the propylene pressure in all experiments was kept constant, increasing the temperature or the trialkylaluminum concentration decreases the *i*PP chain length and vice versa. The overall molecular weight of

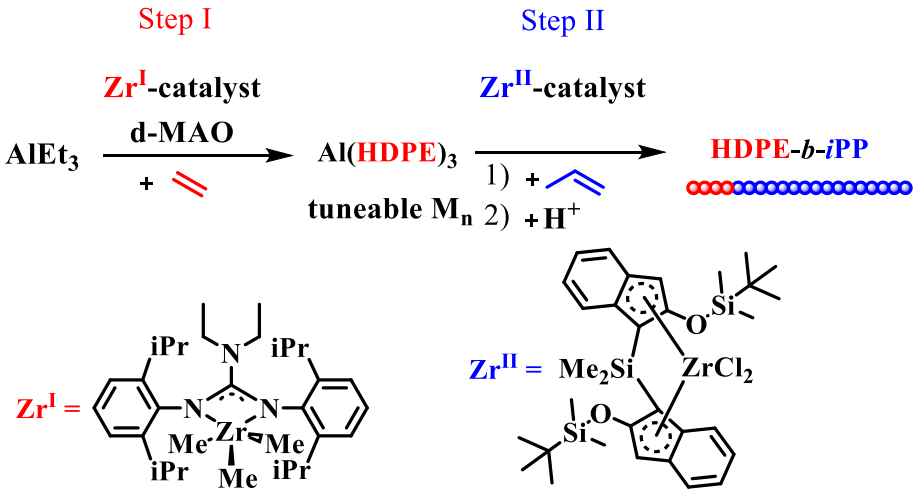

FIGURE 2 | Successive one-pot synthesis of HDPE-*b*-*i*PP diblock copolymers. Step I: Synthesis of Al(HDPE)$_3$. Step II: Elongation of ethylene polymeryl chains with an isotactic polypropylene block.

the diblock copolymers is therefore adjustable by the trialkylaluminum concentration, the ethylene consumption, and the polymerization temperature. Regarding Step II, the inability of Zr^{I} to polymerize pure α-olefins, especially propylene, prevents the formation of atactic polypropylene by-products, whereas Zr^{II} must maintain the irreversibility of the chain transfer even under high $AlEt_3$ concentrations in order to preserve the stereo-control of the copolymer backbone. The remarkable versatility of this dual Zr catalyst system enables the highly efficient synthesis of hard-hard HDPE-*b*-*i*PP diblock copolymers.

Detailed studies about the CCTP of propylene with Zr^{II}, the influence of trialkylaluminum concentration (Table S3, Figure S4), and the polymerization temperature (Table S4, Figures S5—S11) on the molecular weight, the propylene consumption (Table S5 and Figure S12), and trialkylaluminum alkyl chain length (Table S6 and Figure S13) are presented in the Supporting Information. Aluminum termination of all *i*PP chains can be proven either by the absence of olefinic resonances in the high temperature ^{1}H nuclear magnetic resonance (HT-^{1}H-NMR) spectrum of the *i*PP produced at 50°C after acidic workup (Figure S9) or by CCTP of propylene with Zr^{II} followed by oxidation and acidic workup, leading to hydroxy terminated *i*PP (Table S7 and Figure S14). At polymerization temperatures above 80°C, traces of olefinic resonances in the ^{1}H-NMR spectrum (Figure S10) were detected which probably come from decomposition of the sterically crowded Et_2Al*i*PP, whereas Et_2AlHDPE produced with Zr^{II} under the same conditions was stable.

Based on these results, the CCTP of propylene with Zr^{II} starting from Al(HDPE)$_3$ was investigated through continuous sampling during polymerization (Table S8, Figures S16–S20). It was found that as propylene consumption proceeds, the number of elongated polymeryl chains of (HDPE)$_{3-n}$Al(*i*PP-*b*-HDPE)$_n$ ($n = 1$, 2, 3) increased, whereas the molecular weight and the melting point of the *i*PP fraction of the diblock copolymer (Table S14, Figures S21 and S22) remained almost unchanged and independent of the polymerization progress (Figure 3A). This observation proves an irreversible chain transfer process after chain elongation.

After confirming that both catalysts fulfill the requirements, eight different HDPE-*b*-*i*PP diblock copolymers were synthesized (Table 1) following the synthesis protocol outlined in Figure 2. The molecular weight of the aluminum terminated polymers [Al(HDPE)$_3$] was adjusted between 1400 and 2700 g × mol^{-1} [20a], to ensure solubility of the polymer in toluene at 70°C as mentioned above. These long chain aluminum alkyls were then elongated through propylene CCTP at 50°C, 65°C, and 85°C. After quenching the reaction with ethanol/hydrochloric acid, a blend of residual HDPE and HDPE-*b*-*i*PP diblock copolymers was obtained.

2.2 | Characterization of the HDPE-*b*-*i*PP Diblock Copolymers

The polymers were analyzed by high temperature size exclusion chromatography (HT-SEC), differential scanning calorimetry (DSC), solution differential scanning calorimetry (micro-DSC), HT-^{1}H-NMR, and HT-^{13}C-NMR, atomic force microscopy (AFM), and scanning electron microscopy (SEM). HT-SEC gives information about the molecular weight distributions (Table 1, $M_{n\ \mathrm{HDPE}\text{-}b\text{-}i\mathrm{PP}}$) of the HDPE-*b*-*i*PP and the mass fraction (Table 1, $\omega_{\mathrm{HDPE}\text{-}b\text{-}i\mathrm{PP}}$) of elongated HDPE chains. A bimodal molecular weight distribution with slightly overlapping curves (Figure 4) was observed for all samples. Due to this overlap, the HT-SEC curves were deconvoluted into HDPE residue and HDPE-*b*-*i*PP by fitting experimental GPC curves of HDPE/HDPE-*b*-*i*PP blends to two overlapping Gaussian curves (Table 1, Tables S15—S22 and Figures S23—S30) [23]. This method assumes that both polymers exhibit symmetrical curves within the mixture. The low molecular weight fraction ($M_n = 1400$–2400 g × mol^{-1}; $Đ = 1.4$) can be attributed to the unconverted HDPE residue which is comparable to the reference samples of the pure (Table S2; Figure S2) and aliquot HDPE samples taken prior to step 2 (Table S23). The high molecular weight fractions represent the corresponding HDPE-*b*-*i*PP

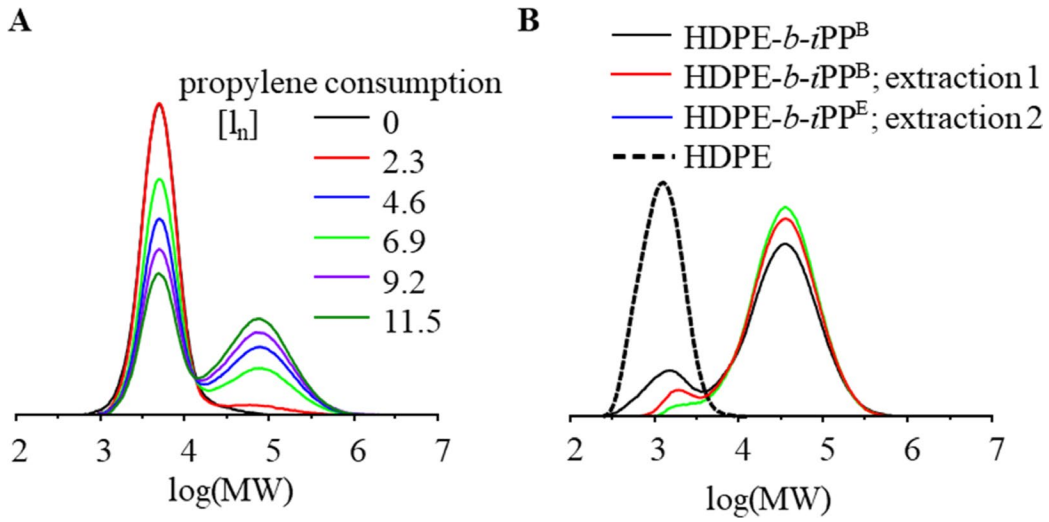

FIGURE 3 | Reaction Monitoring by high-temperature size exclusion chromatography. Molecular weight distributions: (A) Continuous sampling during propylene polymerization (Table S8). (B) Purification of HDPE-*b*-*i*PP from unreacted HDPE through two times Soxhlet extraction of the raw material (Table 1 entry 3b and Tables S23 and S24).

TABLE 1 | Polymerization details for the synthesis of HDPE-*b*-*i*PP using Zr^{I} for ethylene and Zr^{II} for propylene polymerization after activation with *d*-MAO.[a]

Ent.	V_{eth} [l_n]	V_{prop} [l_n]	T_{react}·[°C]	$M_{n\,HDPE}$ [g×mol^{-1}]	$Đ_{PE}$	$M_{n\,HDPE\text{-}b\text{-}iPP}$ [g×mol^{-1}]	$Đ_{HDPE\text{-}b\text{-}iPP}$	$\omega_{HDPE\text{-}b\text{-}iPP}$ [wt.-%]
1	12	—	70	1800	1.4			
		6	50			60,600	2.8	40
2	14	—	70	2200	1.3			
		9	50			54,100	3.4	42
3a[b]	2	—	70	1700	1.5			
		8	50			39,500	2.2	84
3b[c]				3900	1.1	39,500	2.1	98
4	12	—	70	1800	1.4			
		11	65			35,200	1.9	56
5	16	—	70	2700	1.4			
		14	65			31,900	1.9	54
6a	10	—	70	1500	1.4			
		11	65			25,000	2.2	57
6b[c]				2000	1.1	31,300	1.8	81
7a	13	—	70	1500	1.3			
		12	85			11,300	2.1	57
7b[c]				2600	1.1	23,000	1.7	71
8	11	—	70	1400	1.3			
		13	85			10,600	1.9	57

[a]Reaction conditions: $V_{toluene}$ = 250 mL; n_{ZrI} = 1 µmol; n_{ZrII} = 1 µmol; $n_{d\text{-}MAO}$ = 2 mmol; n_{AlEt3} = 2.80 mmol; $p_{ethylene}$ = 3 bara; $p_{propylene}$ = 5 bara; All M_n and the mass ratios were determined by high temperature size exclusion chromatography and subsequent peak deconvolution. Mark-Houwink parameters: K = 40.6 and α = 0.725 for linear HDPE and K = 19.0 and α = 0.725 for *i*PP.
[b]n_{AlEt3} = 1.0 mmol.
[c]HDPE-*b*-*i*PP^{E} after two times Soxhlet extraction.

with an overall M_n ranging from 10,600 to 60,600 g × mol^{-1} and polydispersities typical for metallocene *i*PP of $Đ = 1.9–3.4$. The HDPE-*b*-*i*PP fraction accounts for approximately 40 wt.-%–85 wt.-% of the polymer. The degree of HDPE chain elongation of the aluminum terminated polymer Al(HDPE)$_3$ can be determined by analyzing the amount of HDPE residue compared to the amount of HDPE produced by the ethylene conversion in Step I, which we routinely monitor. Due to the slower chain transfer rate between Zr^{II} and Al(HDPE)$_3$ compared to $AlEt_3$, the molecular weight of the diblock copolymers is significantly higher than pure *i*PP, which was synthesized under the same conditions with $AlEt_3$ as CTA (Table S4).

The melting and crystallization temperatures of HDPE-*b*-*i*PP were determined by DSC measurements (Figures S31—S38). In a typical diblock copolymer raw material (HDPE-*b*-*i*PP^B, B = blend) after polymerization, up to three melting and crystallization peaks can be observed (Figure 5). The DSC curves are composed of residual HDPE, the HDPE-, and the *i*PP-phases of the block copolymer. The assignment of the melting (m.p.) and crystallization (crystn.p.) peaks of the HDPE residue is performed by using reference samples of the pure HDPE, which has a m.p. at 127.8°C and a crystn.p. at 117.5°C (Figure S1). HDPE melting and crystallization temperatures in the mixture were found to be in the range from 120°C to 129°C and between 114°C and 117°C, respectively. The residual melting peaks around 125°C and 145°C, as well as crystallization temperatures of around 110°C and 118°C, were allocated to the HDPE- and the *i*PP-phases of the block copolymer. Both the HDPE- and *i*PP-phases of the block copolymer show lower melting and crystallization temperatures than pure comparative HDPE and *i*PP samples (Figures S1 and S8). The different melting and crystallization temperatures of the HDPE- and the *i*PP-block indicate a microphase separation [24]. To gain more insight and to verify the diblock polymer architecture, three HDPE-*b*-*i*PP^B polymers were two times Soxhlet extracted with benzene at 80°C to remove as much as possible from the residual HDPE. According to HT-SEC measurements (Figure 3B, Figures S39 and S40; Table S24), this results in a decrease of the residual HDPE from 16 wt.-% to 2 wt.-% for entry 3a, from 43 wt.-% to 19 wt.-% for entry 6a, and from 43 wt.-% to 29 wt.-% for entry 7a of Table 1. The extracted HDPE-*b*-*i*PP^E (*E* = extracted) materials were analyzed by high temperature ^{1}H- and ^{13}C-NMR measurements, DSC, micro-DSC, polarization microscopy, and AFM.

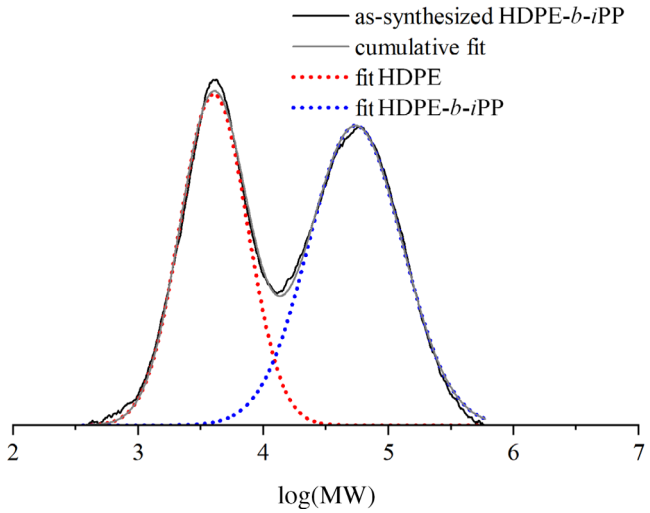

FIGURE 4 | Deconvolution of a typical molecular weight distribution of HDPE-*b*-*i*PP (Table 1, entry 3) determined by high temperature size exclusion chromatography. The red dotted line represents the fit curve of the molecular weight distribution of unreacted HDPE (Mark-Houwink parameters for HDPE: $K = 40.6$ and $\alpha = 0.725$) after the reaction, the blue dotted line represents the fit curve of HDPE-*b*-*i*PP (Mark-Houwink parameters for *i*PP: $K = 19.0$ and $\alpha = 0.725$).

The ^{1}H-NMR (Figure 6, Figures S47 and S50) and ^{13}C-NMR (Figure S48) spectra of the purified polymers Table 1 entry 3b and entry 6b reveal the existence of a HDPE-*b*-*i*PP block copolymer by showing the four resonances of the CH, the two diastereotopic CH_2 and CH_3 protons of the *i*PP as well as the singlet resonance of the CH_2 protons of the HDPE chain [6b, 11, 23b]. By comparing the integrals of PE and polypropylene resonances, the ratio between the *i*PP and HDPE repeating units can be calculated. For the purest HDPE-*b*-*i*PP^E, Table 1 entry 3b, the proportion of HDPE can be determined by this ratio to 11.3 mol-% or 9.3 wt.-% considering the 2 wt.-% of unincorporated HDPE residue. For a detailed calculation, see Table S30.

As expected, the purified diblock copolymers show less melting and crystallization temperatures in the micro-DSC (Figure S51) and DSC as well (Figures 5 and S52—S54). For the purest sample (Table 1 entry 3b), only one melting point in the micro-DSC

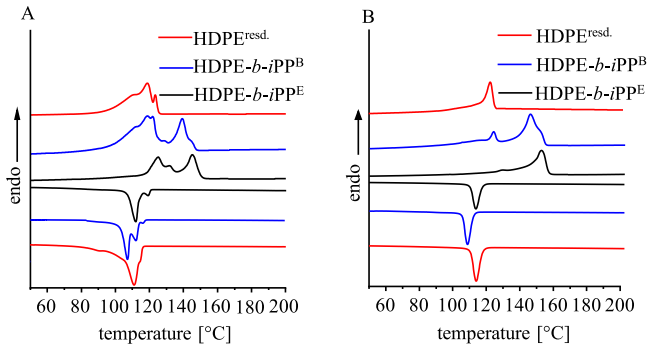

FIGURE 5 | DSC melting and crystallization curves (10 K × min^{-1}) of the extracted HDPE$^{resd.}$, the raw material HDPE-*b*-*i*PP^B and the extracted polymer HDPE-*b*-*i*PP^E for Table 1 entry 6b (A) and entry 3b (B).

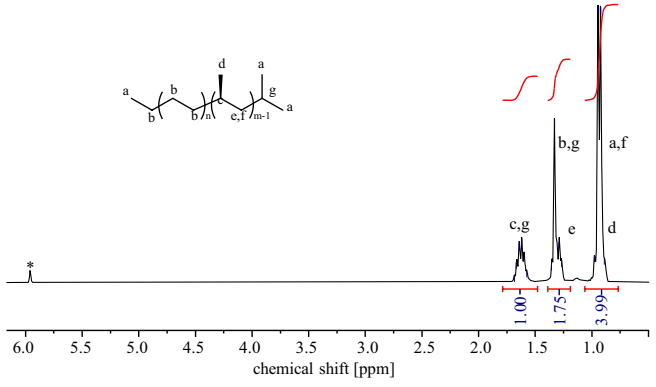

FIGURE 6 | HT-^{1}H-NMR spectrum (300 MHz, 120°C, $C_2D_2Cl_4$) of purified HDPE-*b*-*i*PP^E after 2 × Soxhlet extraction (Table 1, entry 3b); *residual proton resonance of $C_2D_2Cl_4$.

was observed. In contrast, in the DSC, separated melting points at 126.7°C and 148.3°C for the HDPE- and *i*PP-phases were still present, whereas the crystallization point accidentally fell together to one peak at 114.4°C. In addition, polarization microscopy, as well as AFM surface images, show evidence of the presence of a microphase separation. In the micrographs of HDPE-*b*-*i*PP^{E} diblock copolymer recorded with a polarization microscope, the *i*PP block crystallized first on cooling at 135°C to set a hard spherulites morphology in the blend, followed by the lamellar crystallization of HDPE chains (Figure 7 top) [25]. For a detailed temperature profile of the polarization microscopy, see Figure S55.

For AFM, the polymer was dissolved in 1,2,4-trichlorobenzene, and one drop was slowly evaporated at 150°C on an object slide, followed by isothermal crystallization at 130°C. In the AFM micrographs of HDPE-*b*-*i*PP^{E} diblock copolymer (Table 1 entry 3b) a clear phase separation of banded spherulites of HDPE in an *i*PP matrix was observed (Figure 8 left). Banded spherulites of PE have been reported earlier, for example in HDPE-*b*-*a*PP diblock copolymers [26].

2.3 | Compatibilization of *i*PP Containing up to 30 wt.-% HDPE Impurities

The HDPE-*b*-*i*PP^{B} diblock copolymer blends were used as synthesized for compatibilization studies. Dog bone samples of 10/90, 20/80, and 30/70 (wt./wt.) HDPE/*i*PP blends from commercially available HDPE and *i*PP polymers (SABIC HDPE B5823, SABIC PP 500P, Table S1) were prepared and used to determine the mechanical properties by tensile stress–strain measurements. These blends were then compatibilized with 2.5 wt.-%, 5 wt.-%, and 10 wt.-% HDPE-*b*-*i*PP^{B} of different *i*PP

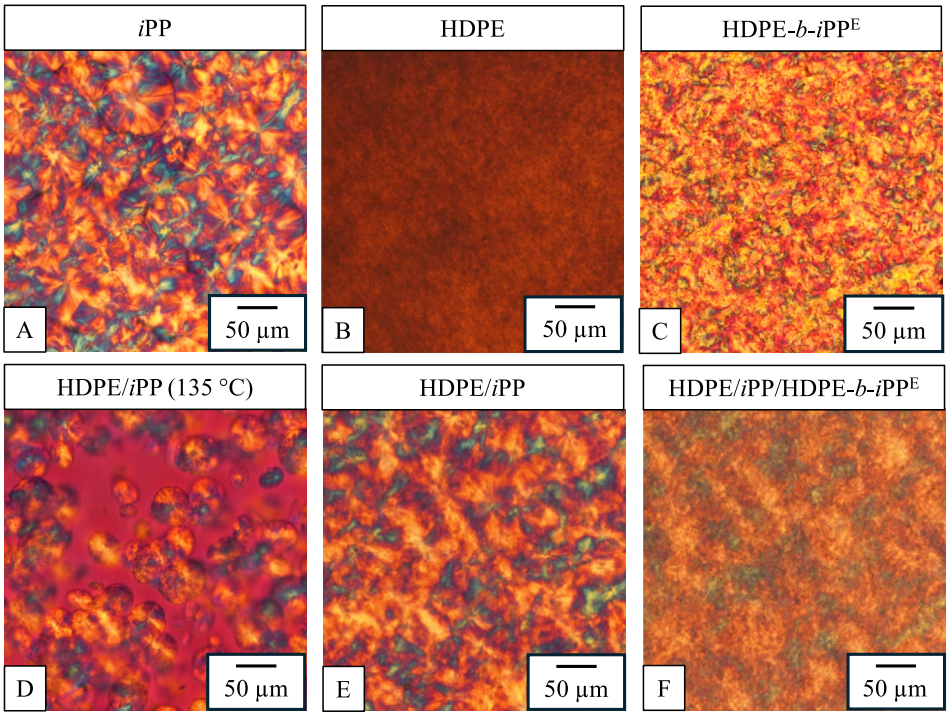

FIGURE 7 | Polarization micrographs after cooling to 25°C of pure *i*PP (A) and HDPE (B), purified HDPE-*b*-*i*PP^{E} (C), neat 30/70 wt.-% HDPE/*i*PP blend (D and E), and compatibilized 27/63/10 wt.-% HDPE/*i*PP/HDPE-*b*-*i*PP^{E} blend (Table 1 entry 6b, F).

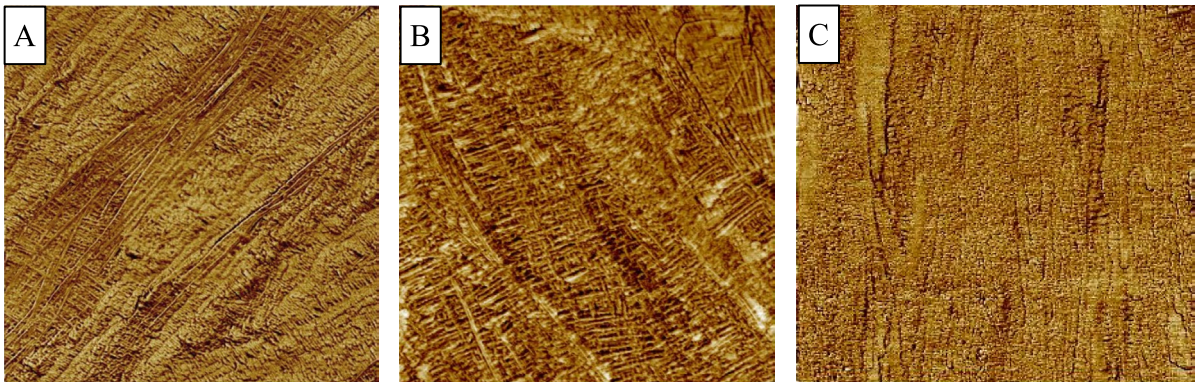

FIGURE 8 | Atomic force microscopy (AFM) micrographs (3 × 3 µm) of neat HDPE-*b*-*i*PP^{E} Table 1 entry 3b, (A) isothermally crystallized at 130°C, 30/70 wt.-% HDPE/*i*PP blend (B) and compatibilized with 10 wt.-% HDPE-*b*-*i*PP^{E} (Table 1 entry 3b, C).

block chain length, and commercial OBC compatibilizers INFUSE™ and INTUNE™. All samples were compared with neat *i*PP and the uncompatibilized blends (Figures S56—S116). The selected results are shown in Figure 9.

A decrease in strain from 252% to 103% by blending *i*PP with 30 wt.-% HDPE can be observed. The addition of 10 wt.-% of HDPE-*b*-*i*PP^{B} to the blend results in an improvement of the average strain in every sample (Table S31) from 119% (Table 1 entry 1) to 458% (Table 1 entry 7a), and matching up with the best commercial OBC compatibilizers INFUSE™ and INTUNE™ [14, 17, 18, 27], which show a restoration of the strain at break for the 30/70 (wt./wt.) HDPE/*i*PP polymer blends to 438% and 447%, respectively. The restoration of the strain at break was found to be inversely related to the *i*PP block chain length or overall molecular weight of the diblock copolymer, with an optimum strain at a weight of 11,300 g × mol^{-1} (Table 1 entry 7a). An additional reduction in molecular weight to 10,600 g × mol^{-1} (Table 1 entry 8) did not further improve the strain but resulted in a slight decrease to 439%. It is noteworthy that the performance of the HDPE-*b*-*i*PP^{B} diblock compatibilizer is closely related to the amount of HDPE in the blend. Although for a 30/70 (wt./wt.) HDPE/*i*PP polymer blend 10 wt.-% compatibilizer is necessary, for 10/90 (wt./wt.) and 20/80 (wt./wt.) HDPE/*i*PP polymer blends 2.5 wt.-% and 5 wt.-% HDPE-*b*-*i*PP^{B} (Table 1 entry 6a, M_n = 25,000 g × mol^{-1}) are sufficient to recover the strain to 451% and 444%, respectively (Figure 10, Table S31).

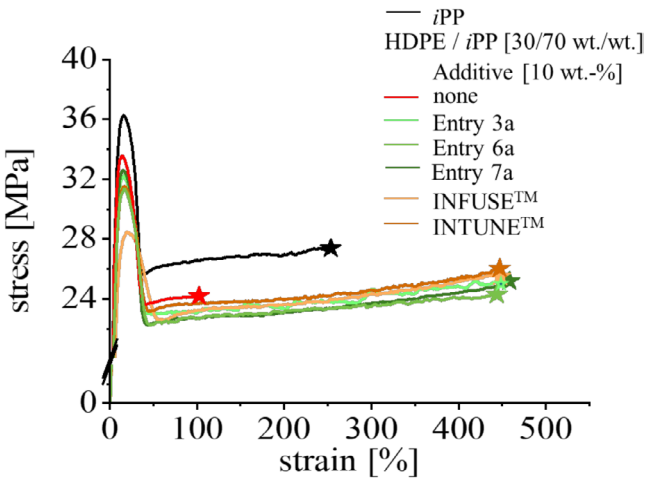

FIGURE 9 | Stress strain plot diagram of *i*PP (black), neat 30/70 (wt./wt.) HDPE/*i*PP blend (red), and compatibilized with 10 wt.-% HDPE-*b*-*i*PP^{B} entry 3a, 6a, and 7a (Table 1), INFUSE™, and INTUNE™.

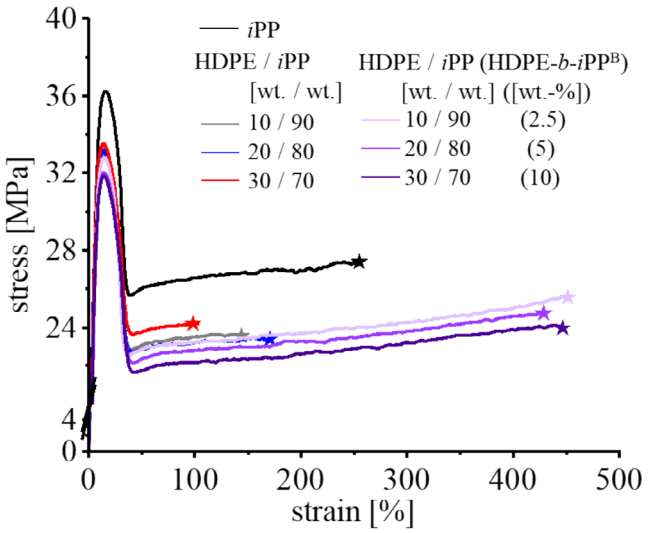

FIGURE 10 | Stress strain plot diagram of *i*PP (black), neat 10/90 (wt./wt.), 20/80 (wt./wt.), and 30/70 (wt./wt.) HDPE/*i*PP blends, and 2.5 wt.-%, 5 wt.-%, and 10 wt.-% HDPE-*b*-*i*PP^{B} compatibilized blends (Table 1 entry 6a, M_n = 25,000 g × mol^{-1}).

After the investigation of the compatibilization ability of the crude HDPE-*b*-*i*PP^{B} diblock copolymers, we became interested in the performance of the extracted HDPE-*b*-*i*PP^{E} ones. Again, dog bones of a 30/70 (wt./wt.) HDPE/*i*PP blend compatibilized with 5 wt.-% and 7.5 wt.-% of HDPE-*b*-*i*PP^{E} of different *i*PP chain lengths were prepared and used for the tensile stress–strain measurements. The results for 5 wt.-% compatibilizer and the comparison with neat *i*PP, INFUSE™, and INTUNE™ are shown in Figure 11.

As expected, the extracted HDPE-*b*-*i*PP^{E} diblock copolymers are highly efficient in the compatibilization of a 30/70 (wt./wt.) HDPE/*i*PP blend. Although for the crude HDPE-*b*-*i*PP^{B} diblock copolymer, 10 wt.-% is necessary to restore the strain at break of a 30/70 (wt./wt.) HDPE/*i*PP blend, for the extracted ones, only 5 wt.-% is needed. The strain was increased to 428%, 438%, and 449% for Table 1 entry 3b, 6b, and 7b, respectively, whereas INFUSE™ and INTUNE™ achieve 342% and 406%, respectively (Table S31). It's noteworthy that HDPE-*b*-*i*PP^{E} diblock copolymers not only restore the strain at break but also do not soften the blend and reduce the stress, like INFUSE™.

2.4 | Investigation of the Compatibilization Mechanism

To get more insight into the compatibilization mechanism of the HDPE-*b*-*i*PP diblock copolymers in HDPE/*i*PP blends, DSC, optical polarization, scanning electron, and atomic

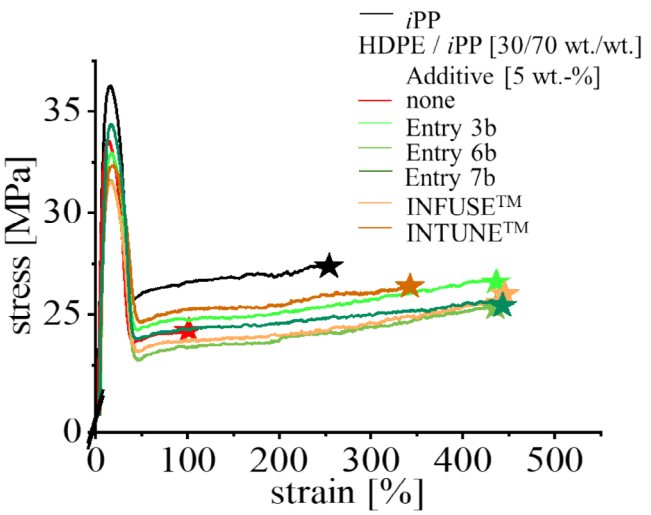

FIGURE 11 | Stress strain plot diagram of *i*PP (black), neat 30/70 (wt./wt.) HDPE/*i*PP blend (red), and compatibilized with 5 wt.-% HDPE-*b*-*i*PP^{E} entry 3b, 6b, and 7b (Table 1), INFUSE™, and INTUNE™.

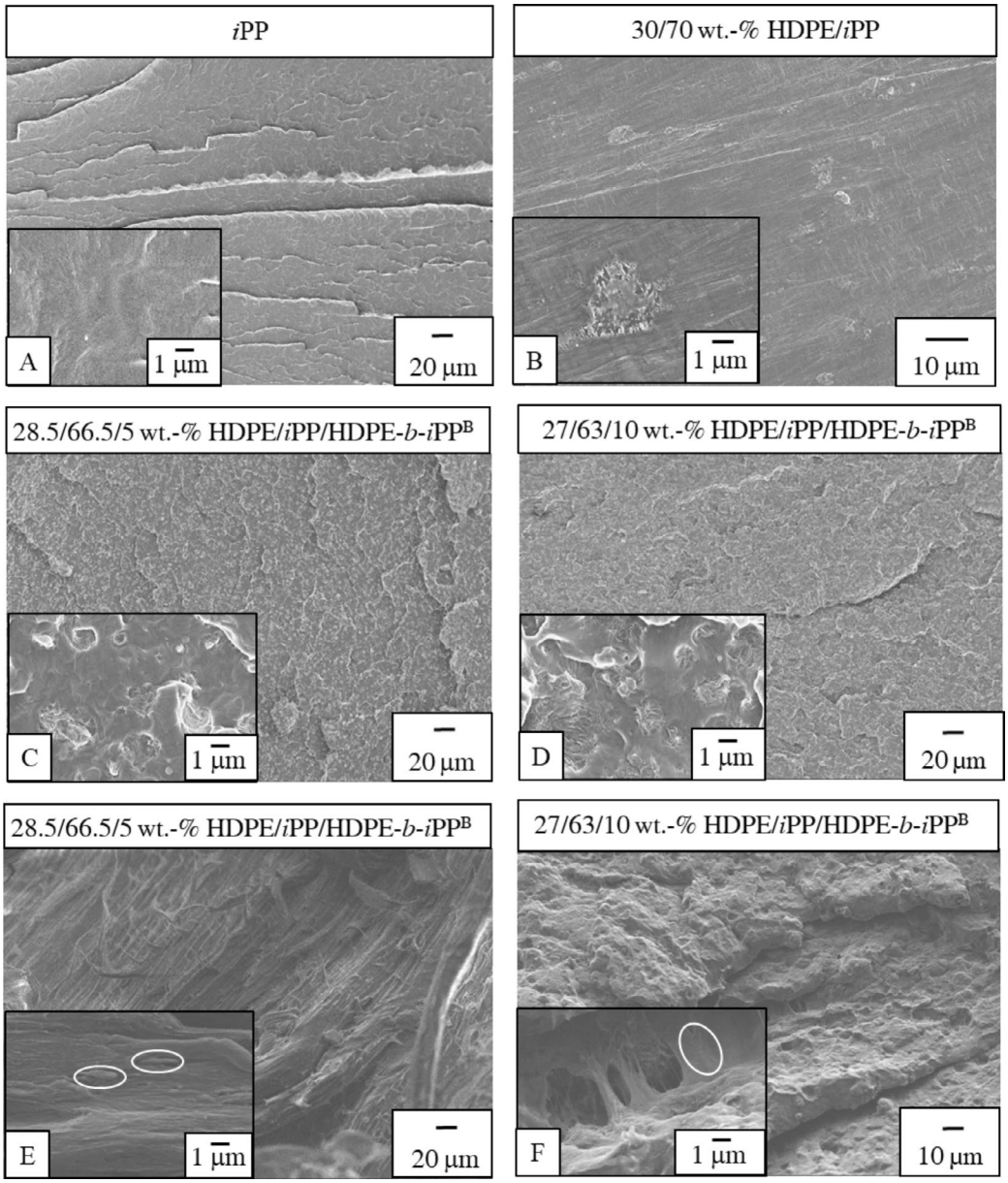

FIGURE 12 | Scanning electron microscopy (SEM) images at different magnifications obtained from injection molded cryo-fractured dog bone specimen cross-sections of: (A) pure *i*PP. (B) 30/70 wt.-% HDPE/*i*PP blend. Compatibilized HDPE/*i*PP/HDPE-*b*-*i*PP^{B} blends with different mass ratios 28.5/66.5/5 wt.-% and 27/63/10 wt.-% before (C and D) and after tensile test (E and F).

force microscopy investigations were performed. For co-crystallization experiments, *i*PP 500P, HDPE B5823, and a 30/70 (wt./wt.) HDPE/*i*PP blend were blended with 10 wt.-% HDPE-*b*-*i*PP^{E} (Table 1 entry 6b) and the DSC melting and crystallization curves were measured (Figures S117—S120). Due to the long *i*PP block chain, HDPE-*b*-*i*PP^{E} (Table 1, entry 6b) and pure *i*PP blends cocrystallize, showing only one melting at 161.0°C (m.p.) and one crystallization point at 116.6°C (crystn.p.). In contrast, pure HDPE and HDPE-*b*-*i*PP^{E} (Table 1, entry 6b) blends display 2 m.p. and 2 crystn.p. indicating HDPE/*i*PP macrophase separation. For a 27/63/10 wt.-% HDPE/*i*PP/HDPE-*b*-*i*PP blend, two melting (131.4°C and 161.4°C) and one crystallization (117.1°C) temperatures are visible.

For the optical polarization microscopy, dynamic crystallization (Temperature profile Figure S55) was performed. The samples were placed between two object slides, melted and tempered at 230°C for 5 min isothermally. A cooling step to 135°C at 10 K × min^{-1} was performed, and the samples were tempered isothermally for 1 h. Crystallization occurs from 135°C to 110°C and is performed at a cooling rate of 5 K × min^{-1}. Afterwards, the samples were cooled to room temperature at a cooling rate of 10 K × min^{-1}. The crystallization of the *i*PP phase in the neat blend 30/70 (wt./wt.) HDPE/*i*PP starts at 135°C and crystallizes in the form of slowly growing spherulites (Figure 7, bottom left). The crystallization of the HDPE phase occurs at 117°C in the form of fast-growing lamella crystals. The HDPE crystals can be identified at the interfaces of the *i*PP spherulite crystals. Below 107°C, a rapid crack formation between the *i*PP spherulites and HDPE lamellas of the neat blend becomes visible. Figure 7, bottom center, shows the blend after finishing the crystallization at 25°C, being permeated by cracks (black) at the spherulite

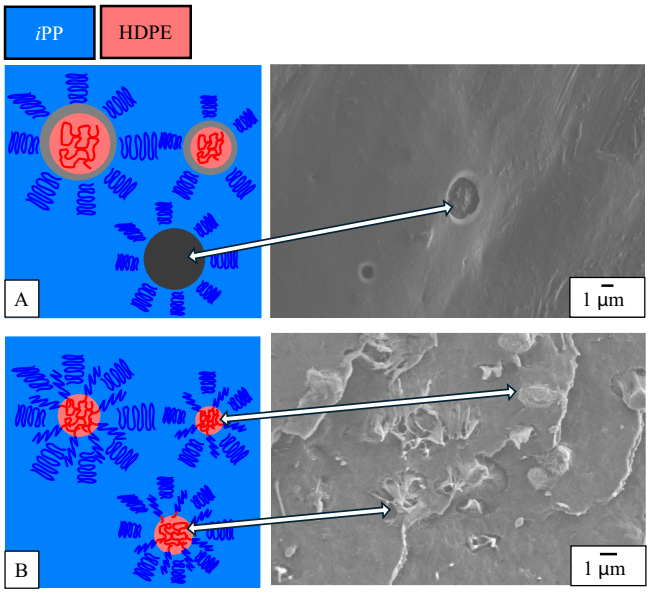

FIGURE 13 | Proposed core shell compatibilization mechanism. (A) A neat 30/70 wt.-% HDPE/*i*PP blend forming large HDPE crystals, which can easily debonded leaving cavities and leading to tensile strength lost. (B) Adding a HDPE-*b*-*i*PP^{B} (blend) diblock copolymer core shell formation anchors the HDPE particles in the *i*PP matrix and restoring the tensile strength.

interphases. The procedure was repeated with the 30/70 (wt./wt.) HDPE/*i*PP compatibilized blend with 10 wt.% HDPE-*b*-*i*PP^{E} (Table 1 entry 6b). No change in the crystallization temperature of the neat polymer phases compared to the pure blend can be observed. The crystalline structure of the blend remained essentially failure-free.

For AFM, the commercial 30/70 wt.-% HDPE/*i*PP blend was dissolved in 1,2,4-trichlorobenzene and one drop was slowly evaporated at 150°C on a glass slide. Similar to the HDPE-*b*-*i*PP^{E} (Table 1 entry 3b) diblock copolymer (Figure 8A), the uncompatibilized blend shows phase separation of the immiscible polymers, resulting in large debonded polymer crystals, leaving cracks between them (Figure 8B). The procedure was repeated by adding 10 wt.-% HDPE-*b*-*i*PP^{E} to the polymer solution, resulting in a shrinkage of the polymer crystals and close packing (Figure 8C).

Phase morphology of immiscible blends is the major determinant of final material properties. Dog bone shaped specimens were prepared by injection molding and investigated by SEM cryo-fractured cross-sections of *i*PP, neat and compatibilized 30/70 wt.-% HDPE/*i*PP blends, before and after tensile testing (Figure 11 and Figures S121—S123).

The SEM images of *i*PP homopolymer (Figure 12A) show large *i*PP crystals in an *i*PP matrix but virtually no cavities, fracture, and so on. The neat 30/70 wt.-% HDPE/*i*PP blend (Figure 11B) exhibits small cracks around the large HDPE crystals, which have weak or loose interactions with the *i*PP matrix and can already be debonded during cryo-fracture, leaving cavities left. The SEM images of compatibilized blends show a decrease in HDPE crystal size by two-thirds and strong HDPE/*i*PP interactions, recognizable by the deformation of the HDPE particles during cryo-fracture. Oval deformation of the HDPE particles can also be observed in Figure 12E,F after tensile testing.

2.5 | Proposed Compatibilization Mechanism

Based on this morphological characterizations and the tensile testing, the following mechanism is proposed. In the 30/70 wt.-% HDPE/*i*PP immiscible blends, large and weakly bonded HDPE particles within the *i*PP matrix were formed, accompanied by crack formation (Figure 13A). This leads to a reduction in the tensile strength by 200% compared to neat *i*PP. By adding the HDPE-*b*-*i*PP^{B} diblock copolymer to the blend, the HDPE particle size decreases by two-thirds and the strain at break was restored. The strong deformation of the HDPE particles after cryo-fracture and tensile testing is the result of the strong anchoring of the particles through the HDPE-*b*-*i*PP diblock copolymer. We propose that the HDPE particles and the compatibilizer form a core shell structure, which is very common for diblock copolymers with a 1/3–2/3 block-to-block chain length ratio [28]. For core shell structures, one very narrowly dispersed block was found to be beneficial [29]. The core shell mechanism is in good agreement with the 3/1 mass ratio of HDPE/HDPE-*b*-*i*PP (core/shell) and the inversely related overall molecular weight of the diblock copolymer for productive compatibilization, because shorter chains can more efficiently cover the HDPE core.

3 | Conclusion

CCTP permits the efficient bulk one-pot synthesis of semicrystalline HDPE-*b*-*i*PP diblock copolymers. Subsequently, operation of two catalysts, with distinct selectivity patterns, enabled a highly flexible synthesis of these diblock copolymers. Variation of the block chain length allows the identification of effective compatibilizers to recycle blends of HDPE and *i*PP. The crude HDPE-*b*-*i*PP^{B} diblock copolymers can be purified by extraction and are competitive or even better than commercially available OBC compatibilizer.

Acknowledgments

We thank the University of Bayreuth and Sasol Germany GmbH for financial support. The authors thank the SABIC Limburg (NL) and DOW Germany for providing the commercially polymer samples. The authors gratefully acknowledge the Keylab "Surface & Interface Characterization" measuring the AFM and SEM samples, and the Keylab "Small Scale Polymer Processing" for dog bone preparation and tensile testing at University of Bayreuth.

References

1. (a) R. Geyer, J. R. Jambeck, and K. L. Law, "Production, Use, and Fate of All Plastics Ever Made," *Science Advances* 7 (2017): e1700782. (b) Plastics Europe, "Plastics—The Fast Facts 2023," 2023, https://plasticseurope.org/knowledge-hub/plastics-the-fast-facts-2023/. (c) D. Jubinville, E. Esmizadeh, S. Saikrishnan, C. Tzoganakis, and T. Mekonnen, "A Comprehensive Review of Global Production and Recycling Methods of Polyolefin (PO) Based Products and Their Post-Recycling Applications," *Sustainable Materials and Technologies* 25 (2020): e00188.

2. (a) T. H. Epps, L. T. J. Korley, T. Yan, K. L. Beers, and T. M. Burt, "Sustainability of Synthetic Plastics: Considerations in Materials Life-Cycle Management," *JACS Au* 2 (2022): 3–11. (b) P. D. Goring and R. D. Priestley, "Polymer Recycling and Upcycling: Recent Developments Toward a Circular Economy," *JACS Au* 3 (2023): 2609–2611. (c) J.-P. Lange, "Managing Plastic Waste—Sorting, Recycling, Disposal, and Product Redesign," *ACS Sustainable Chemistry & Engineering* 9 (2021): 15722–15738. (d) Plastics Europe, "The Circular Economy for Plastics—A European Analysis 2024," 2024, https://plasticseurope.org/knowledge-hub/the-circular-economy-for-plastics-a-european-analysis-2024. (e) T. Thiounn and R. C. Smith, "Advances and Approaches for Chemical Recycling of Plastic Waste," *Journal of Polymer Science* 58 (2020): 1347–1364. (f) I. A. Ignatyev, W. Thielemans, and B. Vander Beke, "Recycling of Polymers: A Review," *ChemSusChem* 7 (2014): 1579–1593. (g) B. D. Vogt, K. K. Stokes, and S. K. Kumar, "Why is Recycling of Postconsumer Plastics so Challenging?," *ACS Applied Polymer Materials* 3 (2021): 4325–4346.

3. (a) D. Nwabunma and T. Kyu, eds., *Polyolefin-Blends* (John Wiley & Sons, Inc., 2008). (b) L. A. Utracki and C. A. Wilkie, *Polymer Blends Handbook: Polyethylenes and Their Blends*, 2nd ed. (Springer Science+Business Media Dordrecht, 2014). (c) J. Karger-Kocsis and T. Bárány, *Polypropylene Handbook: Morphology, Blends and Composites* (Springer, 2019). (d) I. W. Hamley, ed., *Developments in Block Copolymer Science and Technology* (John Wiley & Sons Ltd., 2004). (e) S. Rajan, L. A. Varghese, and S. Joseph, "A Review on Mechanical and Thermal Properties of Binary and Ternary Thermoplastic Immiscible Polymer Blends," *Asian Journal of Applied Science and Technology* 2 (2018): 1021–1028. (f) E. Karaagac, T. Koch, and V.-M. Archodoulaki, "The Effect of PP Contamination in Recycled High-Density Polyethylene (rPE-HD) From Post-Consumer Bottle Waste and Their Compatibilization With Olefin Block Copolymer (OBC)," *Waste Management* 119 (2021): 285–294. (g) T. S. Muzata, L. M. Matuana, M. Rabnawaz, and CRGSC, "Challenges in the Mechanical Recycling and Upcycling of Mixed Postconsumer Recovered Plastics (PCR): A Review," *Current Research in Green and Sustainable Chemistry* 8 (2024): 100407. (h) C. Aumnate, N. Rudolph, and M. Sarmadi, "Recycling of Polypropylene/Polyethylene Blends: Effect of Chain Structure on the Crystallization Behaviors," *Polymers* 11 (2019): 1456.

4. (a) C. Creton, "Molecular Stitches for Enhanced Recycling of Packaging," *Science* 355 (2017): 797–798. (b) C. Koning, M. Van Duin Martin, C. Pagnoulle, and R. Jérôme, "Strategies for Compatibilization of Polymer Blends," *Progress in Polymer Science* 23 (1998): 707–757. (c) A. Graziano, S. Jaffer, and M. Sain, "Review on Modification Strategies of Polyethylene/Polypropylene Immiscible Thermoplastic Polymer Blends for Enhancing Their Mechanical Behavior," *Journal of Elastomers & Plastics* 51 (2019): 291–336.

5. For Recent Reviews on HDPE/iPP Compatibilizer See(a) G. W. Coates, P. D. Hustad, and S. Reinhartz, "Catalysts for the Living Insertion Polymerization of Alkenes: Access to New Polyolefin Architectures Using Ziegler–Natta Chemistry," *Angewandte Chemie International Edition* 41 (2002): 2236–2257. (b) H. Feng, X. Lu, W. Wang, N.-G. Kang, and J. W. Mays, "Block Copolymers: Synthesis, Self-Assembly, and Applications," *Polymers* 9 (2017): 494. (c) M. Karayianni and S. Pispas, "Block Copolymer Solution Self-Assembly: Recent Advances, Emerging Trends, and Applications," *Journal of Polymer Science* 59 (2021): 1874–1898. (d) T.-W. Lin, O. Padilla-Vélez, P. Kaewdeewong, A. M. LaPointe, G. W. Coates, and J. M. Eagan, "Advances in Nonreactive Polymer Compatibilizers for Commodity Polyolefin Blends," *Chemical Reviews* 124 (2024): 9609–9632. (e) S. D. P. Fielden, "Kinetically Controlled and Nonequilibrium Assembly of Block Copolymers in Solution," *Journal of the American Chemical Society* 146 (2024): 18781–18796.

6. For Selected Papers of Diblock Copolymer Compatibilizer See(a) G. J. Domski, J. M. Rose, G. W. Coates, A. D. Bolig, and M. Brookhart, "Living Alkene Polymerization: New Methods for the Precision Synthesis of Polyolefins," *Progress in Polymer Science* 32 (2007): 30–92. (b) C. De Rosa, A. Malafronte, R. Di Girolamo, et al., "Morphology of Isotactic Polypropylene–Polyethylene Block Copolymers Driven by Controlled Crystallization," *Macromolecules* 53 (2020): 10234–10244. (c) Y. Kang, H. Wang, X. Li, et al., "Efficient Preparation of Isotactic Polypropylene-Based Block Copolymers With Tunable Mechanical Properties: From Thermoplastics to Elastomers," *Macromolecules* 57 (2024): 4208–4219.

7. (a) H. Gao, X. Lu, S. Chen, et al., "Preparation of Well-Controlled Isotactic Polypropylene-Based Block Copolymers With Superior Physical Performance via Efficient Coordinative Chain Transfer Polymerization," *Macromolecules* 55 (2022): 5038–5048.For Selected Papers of Triblock Copolymer Compatibilizer See. (b) R. Seguela and J. Prud'homme, "Structural and Mechanical Properties of a Polyethylene-Based Thermoplastic Elastomer," *Polymer* 30 (1989): 1446–1455.

8. For Selected Papers of Linear Multiblock Copolymer Compatibilizer See(a) J. M. Eagan, J. Xu, R. Di Girolamo, et al., "Combining Polyethylene and Polypropylene: Enhanced Performance With PE/i PP Multiblock Polymers," *Science* 355 (2017): 814–816. (b) J. Xu, J. M. Eagan, S.-S. Kim, et al., "Compatibilization of Isotactic Polypropylene (iPP) and High-Density Polyethylene (HDPE) With iPP–PE Multiblock Copolymers," *Macromolecules* 51 (2018): 8585–8596. (c) J. L. Self, A. J. Zervoudakis, X. Peng, W. R. Lenart, C. W. Macosko, and C. J. Ellison, "Linear, Graft, and Beyond: Multiblock Copolymers as Next-Generation Compatibilizers," *JACS Au* 2 (2022): 310–311. (d) Y. Kang, H. Wang, F. Meng, et al., "Upcycling of Polyethylene/Polypropylene Mixtures Promoted by Well-Controlled Multiblock Olefin Copolymers," *Journal of Chemical Engineering* 497 (2024): 155003.

9. For Selected Papers of Star Like Copolymer Compatibilizer See(a) Z. Chen, C. Steinmetz, M. Hu, et al., "Star Block Copolymers at Homopolymer Interfaces: Conformation and Compatibilization," *Macromolecules* 56 (2023): 8308–8322. (b) Z. Ye and R. Subramanian, "Star Polyethylenes by Coordinative Polymerization," *Canadian Journal of Chemical Engineering* 101 (2023): 5162–5178.

10. For Selected Papers of Grafted Copolymer Compatibilizer See(a) A. H. Tsou, C. R. Lopez-Barron, P. Jiang, D. J. Crowther, and Y. Zeng, "Bimodal Poly (Ethylene-Cb-Propylene) Comb Block Copolymers From Serial Reactors: Synthesis and Applications as Processability Additives and Blend Compatibilizers," *Polymer* 104 (2016): 72–82. (b) C. R. López-Barrón and A. H. Tsou, "Strain Hardening of Polyethylene/Polypropylene Blends via Interfacial Reinforcement With Poly(Ethylene-Cb-Propylene) Comb Block Copolymers," *Macromolecules* 50 (2017): 2986–2995. (c) C. R. López-Barrón, P. Brant, M. Shivokhin, et al., "Long-Chain Hyperbranched Comb Block Copolymers: Synthesis, Microstructure, Rheology, and Thermal Behavior," *Macromolecules* 51 (2018): 5720–5731. (d) K. Klimovica, S. Pan, T.-W. Lin, et al., "Compatibilization ofiPP/HDPE Blends With PE-g-iPP Graft Copolymers," *ACS Macro Letters* 9 (2020): 1161–1166.

11. P. Wolff, A. Dickert, W. P. Kretschmer, and R. Kempe, "iPP/PE Multiblock Copolymers for Plastic Blend Recycling Synthesized by Coordinative Chain Transfer Polymerization," *Macromolecules* 55 (2022): 6435–6442.

12. For Selected Papers of Cyclic Copolymer Compatibilizer SeeC. Zou, J. Chen, M. A. Khan, G. Si, and C. Chen, "Stapler Strategies for Upcycling Mixed Plastics," *Journal of the American Chemical Society* 146 (2024): 19449–19459.

13. Sonstige(a) E. Karaagac, T. Koch, and V.-M. Archodoulaki, "Choosing an Effective Compatibilizer for a Virgin HDPE Rich-HDPE/PP Model Blend," *Polymers* 13 (2021): 3567. (b) X. Zhao, H. Li, J. Liu, et al., "One-Step Synthesis of Multi-Block Copolymers of Isotactic Polypropylene (iPP) and Theoretical Studies on the Regioselectivity and Stereoselectivity of Polypropylene," *Journal of Polymer Science* 63 (2025): 1. (c) F. Yu, C. Long, S. Feng, et al., "In-Situ Grafted Ethylene Propylene Diene Monomer (EPDM) Rubber Multiblock Copolymers as Compatibilizers for Polyethylene (PE) and Isotactic Polypropylene (iPP) Blends," *Polymer* 317 (2025): 127959.

14. (a) "Dow Chemical Company, INFUSE 9077 Olefin Block Copolymer," accessed January 8, 2025, https://www.dow.com/en-us/pdp.infuse-9077-olefin-block-copolymer.379760z.html#tech-content. (b) "Dow Effectively Combines PE and PP," 2013, https://www.plasticsto

day.com/packaging/k-2013-dow-effectively-combines-pe-and-pp-talks-packaging-market. (c) S. Vervoort, J. den Doelder, E. Tocha, et al., "Compatibilization of Polypropylene–Polyethylene Blends," *Polymer Engineering and Science* 58 (2018): 460–465. (d) J. Lee, C. L. P. Shan, R. Laakso, L. Madenjian, E. Garcia-Meitin, and M. White, "Polypropylene Based Olefin Block Copolymers for Clear Cold Tough Application," The Dow Chemical Company, accessed March 30, 2025, https://www.eiseverywhere.com/docs/5555/165239. (e) Y. Lin, V. Yakovleva, H. Chen, A. Hiltner, and E. Baer, "Comparison of Olefin Copolymers as Compatibilizers for Polypropylene and High-Density Polyethylene," *Journal of Applied Polymer Science* 113 (2009): 1945–1952. (f) "Accessed January 8, 2025," https://www.facebook.com/DowEurope/videos/infuse-olefin-block-copolymers-enable-the-use-of-recyclable-ployolefin-based-mat/1358267994198902/.

15. For Selected Papers of Chain Shuttling See(a) D. J. Arriola, E. M. Carnahan, P. D. Hustad, R. L. Kuhlman, and T. T. Wenzel1, "Catalytic Production of Olefin Block Copolymers via Chain Shuttling Polymerization," *Science* 312 (2006): 714–719. (b) T. T. Wenzel, D. J. Arriola, E. M. Carnahan, P. D. Hustad, and R. L. Kuhlman, "Chain Shuttling Catalysis and Olefin Block Copolymers (OBCs)," *Topics in Organometallic Chemistry* 26 (2009): 65–104. (c) X. Yin, H. Gao, F. Yang, et al., "Stereoblock Polypropylenes Prepared by Efficient Chain Shuttling Polymerization of Propylene With Binary Zirconium Catalysts and iBu3Al," *Chinese Journal of Polymer Science* 38 (2020): 1192–1201. (d) F. D. Cannavacciuolo, A. Vittoria, C. Ehm, R. Cipullo, and V. Busico, "Polyolefin Chain Shuttling at Ansa-Metallocene Catalysts: Legend and Reality," *European Polymer Journal* 150 (2021): 110396. (e) G. Urciuoli, O. R. de Ballesteros, and F. Auriemma, "Molecular Architecture of Multiblock Copolymers Synthesized by the Chain Shuttling Technology," *Macromolecular Chemistry and Physics* 224 (2023): 2300113.

16. (a) C. Creton, E. J. Kramer, and G. Hadziioannou, "Critical Molecular Weight for Block Copolymer Reinforcement of Interfaces in a Two-Phase Polymer Blend," *Macromolecules* 24 (1991): 1846–1853. (b) C. Creton, E. J. Kramer, H. R. Brown, and C.-Y. Hui, "Adhesion and Fracture of Interfaces Between Immiscible Polymers: From the Molecular to the Continuum Scal," *Advances in Polymer Science* 156 (2001): 53–136.

17. [17] "Dow Chemical Company, INTUNE D5545.00 Olefin Block Copolymer," accessed January 8, 2025, https://resinex.com/de-LU/products/3656-intune-intune-d5545.

18. (a) M. Monti, M. T. Scrivani, and V. Gianotti, "Effect of SEBS and OBC on the Impact Strength of Recycled Polypropylene/talc Composites," *Recycling* 5 (2020): 9. (b) O. R. de Ballesteros, A. Rispo, G. Femina, et al., "Compatibilization of Isotactic Polypropylene (iPP) and Polyethylene (PE) With PP-Based Olefin Block Copolymers," *Polymer* 319 (2025): 128040.

19. For selected reviews of CCTP see(a) R. Kempe, "How to Polymerize Ethylene in a Highly Controlled Fashion?," *Chemistry—a European Journal* 13 (2007): 2764–2773. (b) L. R. Sita, "Ex Uno Plures ("Out of One, Many"): New Paradigms for Expanding the Range of Polyolefins Through Reversible Group Transfers," *Angewandte Chemie International Edition* 48 (2009): 2464–2472. (c) A. Valente, A. Mortreux, M. Visseaux, and P. Zinck, "Coordinative Chain Transfer Polymerization," *Chemical Reviews* 113 (2013): 3836–3857. (d) R. Mundil, C. Bravo, N. Merle, and P. Zinck, "Coordinative Chain Transfer and Chain Shuttling Polymerization," *Chemical Reviews* 124 (2024): 210–244.

20. (a) A. Goller, J. Obenauf, W. P. Kretschmer, and R. Kempe, "The Highly Controlled and Efficient Polymerization of Ethylene," *Angewandte Chemie, International Edition* 62 (2023): e202216464. (b) C. Unger, H. Schmalz, J. Lipp, W. P. Kretschmer, and R. Kempe, "A Closed-Loop Recyclable Low-Density Polyethylene," *Advanced Science* 11 (2024): 2307229. (c) A. Boddien, R. Kempe, W. P. Kretschmer, and J. Obenauf, "Sasol Germany GmbH," Filed May 13, 2015, WO2016180538.

21. R. Leino, H. Luttikhedde, C.-E. Wilén, and J. H. Näsman, "Isospecific Propylene Polymerization With a Novel 2-Substituted Bis(indenyl) Ansa-Zirconocene," *Organometallics* 15 (1996): 2450–2453.

22. For Selected Papers of CCTP With Propylene See(a) R. Leino, H. J. G. Luttikhedde, P. Lehmus, et al., "Homogeneous α-Olefin Polymerizations Over Racemic Ethylene-Bridged Ansa-Bis (2-(Tert-Butyldimethylsiloxy)-1-Indenyl) and Ansa-Bis (2-(Tert-Butyldimethylsiloxy)-4, 5, 6, 7-Tetrahydro-1-Indenyl) Metallocene Dichlorides," *Macromolecules* 30 (1997): 3477–3483. (b) S. Lieber and H.-H. Brintzinger, "Propene Polymerization With Catalyst Mixtures Containing Differentansa-Zirconocenes: Chain Transfer to Alkylaluminum Cocatalysts and Formation of Stereoblock Polymers," *Macromolecules* 33 (2000): 9192–9199. (c) W. Zhang and L. R. Sita, "Highly Efficient, Living Coordinative Chain-Transfer Polymerization of Propene With ZnEt2: Practical Production of Ultrahigh to Very Low Molecular Weight Amorphous Atactic Polypropenes of Extremely Narrow Polydispersity," *Journal of the American Chemical Society* 130 (2008): 442–443. (d) J. Wei, W. Hwang, W. Zhang, and L. R. Sita, "Dinuclear Bis-Propagators for the Stereoselective Living Coordinative Chain Transfer Polymerization of Propene," *Journal of the American Chemical Society* 135 (2013): 2132–2135. (e) A. A. Burkey, D. M. Fischbach, C. M. Wentz, K. L. Beers, and L. R. Sita, "Highly Versatile Strategy for the Production of Telechelic Polyolefins," *ACS Macro Letters* 11 (2022): 402–409.

23. (a) Y. Hu, J. Liu, and W. Li, "Resolution of Overlapping Spectra by Curve-Fitting," *Analytica Chimica Acta* 538 (2005): 383–389. (b) K. J. Goodman and J. T. Brenna, "Curve Fitting for Restoration of Accuracy for Overlapping Peaks in Gas Chromatography/Combustion Isotope Ratio Mass Spectrometry," *Analytical Chemistry* 66 (1994): 1294–1301.

24. (a) L. Leibler, "Theory of Microphase Separation in Block Copolymers," *Macromolecules* 13 (1980): 1602–1617. (b) Y. Matsushita, "Microphase Separation (Of Block Copolymers)," in *Encyclopedia of Polymeric Nanomaterials*, ed. S. Kobayashi and K. Müllen (Springer, 2014). (c) A. Z. Panagiotopoulos, "Solvent Selectivity Controls Micro-Versus Macrophase Separation in Multiblock Chains," *Macromolecules* 57 (2024): 8253–8261. (d) A. Cicolella, F. De Stefano, M. Scoti, et al., "Phase Separation and Crystallization in Monodisperse Block Copolymers of Linear Low-Density Polyethylene and Isotactic Polypropylene," *Macromolecules* 57 (2024): 2230–2245. (e) H. Jones, J. McClements, D. Ray, M. Kalloudis, and V. Koutsos, "High-Density Polyethylene–Polypropylene Blends: Examining the Relationship Between Nano/Microscale Phase Separation and Thermomechanical Properties," *Polymers* 17 (2025): 166. (f) A. Grzyb, J. S. Kłos, A. Erbaş, M. Lang, and J. Paturej, "Lamellar Domain Spacing of Copolymers With Nonlinear Block Architectures," *Macromolecules* 58 (2025): 1521–1536.

25. Spherical Lamellar(a) M. Ueda, K. Sakurai, S. Okamoto, et al., "Spherulite Formation From Microphase-Separated Lamellae in Semi-Crystalline Diblock Copolymer Comprising Polyethylene and Atactic Polypropylene Blocks," *Polymer* 44 (2003): 6995–7005. (b) B. Crist and J. M. Schultz, "Polymer Spherulites: A Critical Review," *Progress in Polymer Science* 56 (2016): 1–63. (c) C. de Rosa, R. di Girolamo, A. Malafronte, et al., "Polyolefins Based Crystalline Block Copolymers: Ordered Nanostructures From Control of Crystallization," *Polymer* 196 (2020): 122423.

26. (a) S. Kanomi, H. Marubayashi, T. Miyata, and H. Jinnai, "Reassessing Chain Tilt in the Lamellar Crystals of Polyethylene," *Nature Communications* 14 (2023): 5531. (b) Q. Zhang, J. Fan, and J. Feng, "Formation of Banded Spherulites and the Temperature Dependence of the Band Space in Olefin Block Copolymer," *RSC Advances* 5 (2015): 43155–43163. (c) Y. J. Lee, C. R. Snyder, A. M. Forster, M. T. Cicerone, and W.-L. Wu, "Imaging the Molecular Structure of Polyethylene Blends With Broadband Coherent Raman Microscopy," *ACS Macro Letters* 1 (2012): 1347–1351. (d) E. M. Woo and G. Lugito, "Origins of Periodic Bands in Polymer Spherulites," *European Polymer Journal* 71 (2015): 27–60.

27. (a) Z. Zhang, F. Yu, N. Zhou, and H. Zhang, "Compatibilization by Olefin Block Copolymer (OBC) in Polypropylene/Ethylene-Propylene-Diene Terpolymer (PP/EPDM) Blends," *Journal of Macromolecular Science, Part B: Physics* 54 (2014): 159–176.

28. Core Shell Diblock(a) A. Milchev, A. Bhattacharya, and K. Binder, "Formation of Block Copolymer Micelles in Solution: A Monte Carlo Study of Chain Length Dependence," *Macromolecules* 34 (2001): 1881–1893. (b) C. Guerrero-Sanchez, D. Wouters, C.-A. Fustin, J.-F. Gohy, B. G. G. Lohmeijer, and U. S. Schubert, "Structure–Property Study of

Diblock Copolymer Micelles: Core and Corona Radius With Varying Composition and Degree of Polymerization," *Macromolecules* 38 (2005): 10185–10191. (c) C. Pierleoni, C. Addison, J.-P. Hansen, and V. Krakoviack, "Multiscale Coarse Graining of Diblock Copolymer Self-Assembly: From Monomers to Ordered Micelles," *Physical Review Letters* 96 (2006): 128302. (d) R. A. Ramli, W. A. Laftah, and S. Hashim, "Core–Shell Polymers: A Review," *RSC Advances* 3 (2013): 15543. (e) E. Wang, J. Lu, F. S. Bates, and T. P. Lodge, "Effect of Corona Block Length on the Structure and Chain Exchange Kinetics of Block Copolymer Micelles," *Macromolecules* 51 (2018): 3563–3571. (f) L. Qi, L. Wu, R. He, H. Cheng, B. Liu, and X. He, "Synergistic Toughening of Polypropylene With Ultra-High Molecular Weight Polyethylene and Elastomer-Olefin Block Copolymers," *RSC Advances* 9 (2019): 23994–24002. (g) F. Li, Y. Gao, Y. Zhang, and W. Jiang, "Design of High Impact Thermal Plastic Polymer Composites With Balanced Toughness and Rigidity: Toughening With Core-Shell Rubber Modifier," *Polymer* 191 (2020): 122237.

29. (a) S. T. Trzaska, L.-B. W. Lee, and R. A. Register, "Synthesis of Narrow-Distribution "Perfect" Polyethylene and Its Block Copolymers by Polymerization of Cyclopentene," *Macromolecules* 33 (2000): 9215–9221. (b) S. Park, D. Y. Ryu, J. K. Kim, M. Ree, and T. Chang, "Property of Diblock Copolymer Having Extremely Narrow Molecular Weight Distribution," *Polymer* 49 (2008): 2170–2175.

Supporting Information

Additional supporting information can be found online in the Supporting Information section.